CONTRACT # DE-AC02-76-CHO-3073

PPPL--1958

DE83 003899

X-RAY DIAGNOSTICS FOR TFTR*

S. von Goeler, K.W. Hill, M. Bitter, C. Clifford, E. Fredd, M. Goldman, L.C. Johnson, L.P. Ku, E. Moshey, G. Renda, N. Sauthoff, S. Sesnic,** F. Tenney, and K.M. Young

Princeton University, Plasma Physics Laboratory

Princeton, New Jersey 08544

ABSTRACT

A short description of the X-ray diagnostic preparation for the TFTR tokamak is given. The X-ray equipment consists of the limiter X-ray monitoring system, the soft X-ray pulse-height-analysis-system, the soft X-ray imaging system and the X-ray crystal spectrometer. Particular attention is given to the radiation protection of the X-ray systems from the neutron environment.

*Presented at the Course and Workshop, "Diagnostics for Fusion Reactor Conditions," Varenna (Como) Italy, Sept. 6-17, 1982.

**On leave from the Max Planck Institut für Plasmaphysik, Garching near Munich, Germany.

This paper gives a short description of the X-ray diagnostic preparation for the Tokamak Fusion Test Reactor (TFTR), the very large tokamak which will begin operation in Princeton at the end of the year 1982. Basically, the X-ray diagnostics for TFTR make use of techniques which have been proved on earlier tokamaks and have been developed to a high degree of perfection on PLT and PDX /1/2/. This gives us an opportunity in this lecture to briefly review the standard X-ray techniques used on tokamaks. Many new features have been incorporated into the design of the TFTR X-ray diagnostics, which probably represent the most sophisticated X-ray system installed on a tokamak, and in the course of the lecture we shall point out these improvements. The real challenge for the TFTR X-ray diagnostics development, however, has arisen from the fact that TFTR will be the first tritium-burning tokamak and that TFTR will produce a neutron flux almost as large as the neutron flux in a fusion reactor. Since the neutron flux is accompanied by a comparable γ-ray flux, it is evident that the X-ray diagnostics are particularly vulnerable to noise generated by the neutrons. A large part of the paper will be devoted to a discussion of how to cope with neutrons /3/.

A first taste of the neutron problem was obtained already on PLT and PDX during neutral-beam heating of deuterium plasmas with deuterium beams. The injected 40 to 50 keV deuterium ions produced sufficient neutrons to put many of the X-ray detectors out of operation. Figure 1 shows the noise pulses generated by neutrons in one of the liquid-nitrogen cooled lithium drifted silicon detectors on PLT. For these shots the soft X-ray aperture in front of the Si(Li) detector was reduced to the smallest possible area so that the detector response was due almost exclusively to neutron noise. Neutral-beam heating took place in the time interval from t = 400 ms to 600 ms, and neutron

detectors /4/ indicated a total neutron production of 1×10^{13} neutrons/sec during heating (Fig. 1a). The count rate generated by the neutrons in the Si(Li) detector (Fig. 1b) is, under these conditions, comparable in magnitude to the highest normal X-ray count rate of 40 kHz. The flat spectrum of pulses that the neutrons generate in the Si(Li) detector is shown in Fig. 1c. It is produced by silicon recoils from elastic and inelastic scattering of neutrons with atoms of the detector, and also by Compton electrons generated in the detector by γ rays from (n, γ) reactions. The largest neutron yields measured on PLT and PDX have been 2×10^{14} and 3×10^{14} neutrons per sec, respectively, and as a consequence the data from the pulse-height-analysis system were virtually drowned in neutron noise during discharges which were of greatest interest. The situation was even worse for the multiwire proportional counter used as a position sensitive detector in the X-ray crystal spectrometer, since this detector has a much larger sensitive area than the Si(Li) detector. In principle, the neutron noise can easily be avoided by proper shielding, although it turned out in practice that there was often not enough room left around a diagnostic to install the very bulky and voluminous neutron shielding.

Neutron shielding consists of three components: (1) The neutrons are slowed down either by inelastic or elastic scattering in a moderator, consisting of a hydrogen-rich substance like paraffin, polyethylene, water, or concrete. For neutrons with energies of several MeV (e.g., 14 MeV d-t neutrons) the elastic cross section of hydrogen becomes small, and a layer of steel or zinc can be added in front of the hydrogen-rich material in order to slow down the neutrons by inelastic scattering from 14 MeV to 1 to 2 MeV; this produces, however, many γ-rays. (2) Once the neutrons are slowed down, they

are absorbed by a material with a large cross section for thermal neutrons, e.g., lithium or boron. Neutron absorption in lithium does not produce any X rays and neutron absorption in boron produces only X rays of relatively low energy (450 keV). (3) Finally, the γ rays, which stem from (n, γ) reactions and which roughly equal the neutrons in number, have to be shielded out by a good X-ray absorber like lead.

The properties of some practical shielding materials are listed in Table 1. Borated polyethylene is probably the most efficient shielding material for (d,d) neutrons, but it is relatively expensive and presents a safety hazard because it is inflammable. Figure 2 shows the reduction in neutron noise that can be obtained by a combination of borated polyethylene and lead shielding. The calculation /5/6/ assumes that the neutron and γ-ray fluxes which impinge on the shielding are isotropic and that the energy distribution of the neutrons and γ rays is identical to the one shown in Fig. 3. A shield constructed according to these principles, consisting of 20 cm of polyethylene containing 5% boron and 10 cm of lead, provided satisfactory protection for the multiwire proportional counter on PDX. In order to reduce the neutron flux by factors of a hundred to a thousand, the shield has to be meticulously closed around the detector, and the opening where the X rays enter has to have a long collar of shielding material, thereby reducing the solid angle of the aperture.

For TFTR, the neutron-production rate with 40 MW deuterium injection into a tritium plasma is projected to be $\sim 10^{19}$ neutrons/sec with energies of 14 MeV instead of 2.45 MeV. At first sight it would seem an almost hopeless undertaking to perform X-ray measurements under these circumstances. However,

X-ray experiments seem still possible thanks to a special feature of TFTR, namely, the diagnostic basement. Figure 3 shows neutron and γ-ray fluxes calculated by Long-Poe Ku /7/ for TFTR at various locations. The figure demonstrates the very large reduction of neutron flux in the basement of TFTR, which makes X-ray measurements possible even during the d-t phase of operation.

There are presently four X-ray diagnostic systems under preparation for TFTR which will now be discussed in detail.

I. The limiter hard X-ray monitoring system (HX).

This system is designed to measure the hard X-ray bremstrahlung produced by runaway electrons on the limiter. The hard X-ray detectors serve mainly to warn the machine operators of excessive runaway production and possible imminent damage to limiters and vacuum vessel. The TFTR system consists of several 2" x 2" sodium iodide NaI(Tl) and plastic scintillators mounted in the neighborhood of the limiter. Similar detection schemes are used on practically all tokamaks. Usually the measurements are not made in a quantitative way. During neutral-beam heating, in particular during d-t operation, detector noise caused by neutrons will be overwhelming. However, it is presently assumed that monitoring of the runaway level before and after heating suffices.

II. The soft X-ray pulse-height-analysis system (PHA).

A schematic drawing outlining the principle functions of the PHA system /8/ is shown in Fig. 4. An X-ray photon creates electron-hole pairs in the liquid-nitrogen cooled, lithium drifted silicon detector /9/. The number of

charge pairs is proportional to the energy of the photon (3.63 eV photon energy per electron-hole pair). The charges are detected by a charge-sensitive preamplifier. The preamplifier is an integrator, and every photon creates a negative voltage step (see insert in Fig. 4). When the output voltage approaches -5 volts, the preamplifier is reset to -1 V by the reset transistor. (Most commercial systems use either resistive feedback or optical reset, i.e., during the reset, light from an LED illuminates the input FET.) The input FET and the reset transistor are located in the cryostat and are kept at liquid-nitrogen temperature in order to minimize electrical noise. The shaping amplifier creates electrical pulses from the voltage steps. The pulse height is proportional to the photon energy. Each shaping amplifier contains actually two branches. A slow amplifier with a peaking time of 3.9 μs has good energy resolution and produces the pulses that are digitized in the analog-to-digital converter (ADC) and form the photon energy spectrum. The fast amplifier with a peaking time of either 60, 150 or 450 ns detects the presence of a photon. It triggers the pulse-pile-up logic circuits that reject unwanted double pulses. It also provides the input for the scaler, which measures the count rate, the quantity needed for making deadtime corrections. The photo inserted in Fig. 4 shows the six-detector cryostat developed and built by Lawrence Radiation Laboratory, Berkeley specifically for TFTR /10/. (The seventh beryllium window shown on the photo is for energy calibration of the detectors with a radioactive source.)

The physical layout of the PHA system for TFTR is given in Fig. 5. The drawing shows 12 arms (each with six detectors) which are located in the diagnostic basement and look vertically through the plasma; because of financial constraints, the system is presently limited to six arms. Each arm contains

(a) three drives with several foil sets /8/ used to control the energy region over which a detector samples,

(b) a drive with several aperture sets used to control the count rate,

(c) a drive with several sets of neutron collimators /11/12/ used to limit the number of direct 14 MeV neutrons,

(d) lead and borated polyethylene shielding used to keep out neutrons and X rays from the background in the diagnostic basement.

Compared with the PDX system, the TFTR pulse-height-analysis system possesses a number of improvements. We want to list these improvements now and also discuss the radiation aspects of the system:

(1) Time resolution. The group at Lawrence Berkeley Laboratory /10/ which built the Si(Li) detectors has optimized the amplifiers-in particular, the pulse shaping networks of the fast amplifier and the pulse-pile-up logic-so that count rates of 100 kHz (as compared to 40 kHz for the PDX system) seem feasible. The increase in number of detectors from 3 to 6 might also result in improved time resolution.

(2) Dynamic range of electron temperature. During neutral-beam heating, the electron temperature is expected to increase considerably in TFTR. This causes difficulties because the count rates tend to increase dramatically when the temperature rises. The six detector system will be split up so that three detectors are optimized to take data during heating, while the remaining three take data before and after heating.

(3) Extension of electron-temperature range. The 3 mm thick Si(Li) detectors become transparent to X-ray photons with energies larger than 25 keV. A germanium detector is incorporated among the six detectors, extending the photon energy range to 90 keV. This feature should permit reliable measurement of electron temperatures in excess of 10 keV.

(4) Radiation aspects. In order to provide radiation protection, the detectors are placed in the diagnostic basement with 6 feet of concrete between them and the machine. Even there, additional shielding of lead and borated polyethylene is required in order to keep out the neutrons and γ rays from the background radiation of the diagnostic basement (Fig. 5). This shielding is necessary also for d-d operation during the time before installation of the igloo.

A further problem is created by direct 14 MeV neutrons from the plasma. In order to minimize the number of neutrons, neutron collimators /11/ .2/ are inserted which have nearly the same opening as the X-ray apertures. Even so, about 2×10^5 neutrons per sec are projected to strike the detectors which measure the high energy portion of the X-ray spectrum. It is imperative that the direct neutrons strike only the detector and not the supporting structure or the cold finger behind the detector. The Berkeley detector is specifically constructed to give the neutron beam an unobstructed path through the cryostat. Even so, the remaining 2×10^5 neutrons will generate 5400 counts in a 3 mm thick silicon detector, and this represents a strong noise source which will be discussed now.

The various cross sections for 14 MeV neutrons in silicon are given in Table II. Forty-five percent of the counts result from elastic collisions between neutrons with silicon atoms and are produced by silicon recoils. According to the billiard-ball model, the silicon recoils have a relatively flat energy spectrum which extends up to 1.9 MeV. Measured differential cross sections /14/ show a peaking at small angles, which shifts the silicon recoil energy distribution somewhat toward lower energies. Only a fraction of the recoil energy goes into ionization /15/. This fraction, i.e., the ionization produced by a recoil relative to the ionization produced by an electron of equal energy, ranges from a value of 0.3 at 20 keV to a value of 0.9 at 1.9 MeV. The effect on the pulse-height distribution generated by the recoils in the Si(Li) detector will be an increase in the number of smaller pulses and a reduction of the number of larger pulses. According to Table II inelastic collisions are also very important. They give rise to a silicon recoil spectrum of similar shape. The (n,p) and (n,α) reactions, shown in Table II, are fewer in number than the (n,n) reactions /16/. However, they generate pulses which are considerably larger than the pulses from (n,n) and (n, n') reactions. The protons and α-particles deposit essentially their full energy into ionizations. Since the threshold for the dominant isotope Si^{28} occurs at 3.867 MeV for the (n,p) reaction, and at 2.663 MeV for the (n,α) reaction /17/, one expects to see pulses with energies of up to about 11 MeV. For Si^{29} with an abundance of 4.7% in natural silicon, the Q-value for the (n,α) reaction is only 0.021 MeV /17/18/, so that even a few 14 MeV pulses might occur. Most of the pulses created then by direct neutrons in the detectors are so large that they can be

eliminated by an upper level pulse discriminator; the remainder will make up a small background that has to be subtracted.

The very large pulses from (n,p) and (n,α) reactions create an additional problem because they saturate the amplifiers. The fast transistor reset developed by Berkeley resets the preamplifiers in 10 μs /19/, and special clamping and gated baseline restoring circuits have been added to the shaping amplifiers to prevent overloading from large pulses. The system was tested with 2.3 MeV β^- radiation from a (Sr^{90}, Y^{90}) source in order to demonstrate that the very large pulses generated by the 14 MeV neutrons do not block the electronics and interfere with the measurement of X rays in the neighborhood of a few keV. It should be noted that no detector damage is expected from the 14-MeV neutrons. There are presently only 4000 tritium discharges allowed in TFTR, and these last for less than one second each. The maximum neutron fluence through the Si(Li) detectors is then $4 \cdot 10^9$ neutrons per cm^2, which is about a factor 3 to 4 below the Si(Li) damage threshold /20/21/.

III. The soft X-ray imaging system (XIS).

A schematic drawing which outlines the principle functions of the XIS system /22/ is shown in Fig. 6. X-ray photons again produce electron-hole pairs in a silicon detector. Instead of considering single photons, however, we now let very many photons pass through a filter foil onto the detector and register the current in the detector with a sensitive current preamplifier. The objective is to measure fast changes of the total X-ray emission in order to diagnose the position of the plasma column, its shape, or the characteristics of plasma instabilities. The bandwidth of the current

preamplifier is 600 kHz, and the noise current is 1.6 nA rms with a 60 pF input capacitance. Detector leakage current is compensated in this preamp before each shot. The current is recorded by a transient recorder that consists of an amplifier with remotely controlled gain and anti-aliasing filtering, an ADC, clock and memory. The analyzer has two branches, a slow digitizer for recording the whole discharge and a fast burst digitizer for time intervals of special interest. The photo inset shows a silicon surface barrier module for TFTR.

Figure 7 illustrates the physical layout of the XIS system. The silicon surface barrier detectors are mounted in two linear arrays: a horizontal array consisting of two rows of 38 detectors each, and an almost identical vertical array. Because of financial cutbacks, only fifty of the 76 detectors of each array will be instrumented, and the construction of a second vertical array has been halted. Basically, these arrays form pin-hole X-ray cameras which take a few thousand "pictures" at time intervals as small as a few microseconds. Because the plasma emission in a tokamak does not vary significantly along the magnetic field, linear arrays are sufficient, and the pinhole consists actually of a slot hole, aligned parallel to the magnetic field. Under normal conditions the plasma rotates in the poloidal direction, and, as a consequence, techniques employed in X-ray tomography /23/ can be used to reconstruct the X-ray emission from a plasma cross section. Lines of equal plasma emission are interpreted as magnetic surfaces. These techniques have been developed to a high degree of perfection on the PLT and the PDX tokamaks.

It should be stressed that the previously discussed system is <u>not</u>(!) tritium compatible, and we now have to outline the TFTR philosophy for X-ray imaging. The main benefit of this system for TFTR will be that it allows

detailed MHD analysis. In particular, it is considered indispensible for the analysis of instabilities in plasmas with very high temperature and very high β, which TFTR is projected to generate. Since the β value of the tritium plasmas is not expected to be substantially different from the β value in deuterium plasmas, the MHD information can probably be gained during deuterium operation. Even during d-d operation, however, the neutron flux is so large that the system requires shielding by 50 cm borated polyethylene and 15 cm of lead. Without shielding the silicon surface barrier detectors would suffer permanent damage /24/25/ after a few hundred full power deuterium shots. During d-t operation the detectors will be destroyed even faster, namely after 50 shots, even in the presence of shielding. As a countermeasure, ionization chambers /26/ have been developed (Fig. 8). These do not suffer any permanent damage and will take the place of the silicon detectors during d-t operation. The ionization chambers, although they give signals very similar to those of the silicon detector, have a few drawbacks which prevent us from installing them immediately on TFTR. These objectionable features follow:

(a) Although the ionization chamber suffers no damage, neutron noise precludes their use during d-t shots. (This is, of course, also the case for silicon detectors.)

(b) The area of the ionization chamber is larger than the area of the silicon detector by the ratio of the ionization yield ($\approx$ 30 eV/ion pair) in argon to the ionization yield in silicon (3.63 eV/ion pair). This means that the number of detectors has to be reduced when we go to the ionization chambers.

(c) There exists a window problem for the ionization chambers. The gas pressure in the chamber amounts to several 100 Torr, and, therefore,

relatively thick entrance windows are required. There is also a "dead-layer" directly behind the window where no electric field is applied and where no charges are collected. This dead layer acts as an X-ray filter. The research on ultra soft X-ray radiation /29/ will be strongly impeded with the ionization chamber.

In the long run, one would like to install a diagnostic that works well during d-t operation. The work on the rotating crystal spectrometer, which will be discussed in the lecture on X-ray spectroscopy /30/, shows quite some promise in this respect, since X-ray diffracting crystals provide a means of removing the detector from the intense direct neutron beam produced by the plasma.

IV. The X-ray crystal spectrometer (XCS)

The design of the X-ray crystal spectrometer for TFTR has not been finalized yet, and, as a consequence, we can only give here a short outline of the plans which are presently under discussion. It is expected that these plans will undergo several modifications before construction starts.

The principle of the measurement /31/32/33/ is illustrated in Fig. 9. X rays from a tokamak plasma are reflected from a crystal if they meet the Bragg condition

$$\lambda = 2d \sin \theta,$$

where λ is the wavelength, d the spacing between atomic planes of the crystal and θ the Bragg angle. Since the crystal is curved, the X-rays are focused on the Rowland circle. The focused radiation is detected with a position-sensitive multiwire proportional counter. The X-ray spectroscopy of highly ionized atoms has witnessed an astonishing and fascinating development during the last few years, and we will devote another lecture /30/ to the discussion of the physics of this diagnostic.

A proposed physical layout of the X-ray crystal spectrometer is shown in Fig. 10. There are several crystals and multiwire-proportional counters operating simultaneously. Financial cutbacks presently restrict the number of arms to three. It is hoped that we will be able to install more detectors later and that we will be able to measure the line radiation as a function of radius. After all, for the high density operation of TFTR the crystal-spectrometer is expected to be the main ion-temperature diagnostic /32/. The plane of the spectrometer is inclined by an angle of 4.5° with respect to a vertical view in order to measure the Doppler shift of line radiation due to toroidal rotation of the plasma. The indicated shielding of the detectors by 15 cm borated polyethylene and 15 cm lead is sufficient for d-d operation. Much heavier shielding and smaller detectors will be used during d-t operation.

We conclude our short discussion of the XCS system by listing the improvements which will be incorporated in the TFTR design:

(a) The XCS system will have improved time resolution. This is achieved by the following features:

(1) Multiwire proportional detectors with count rate capabilities of

350 kHz have been developed by Padeka and his group /33/ at Brookhaven National Laboratory. The recent electronic development of time-to-digital converters (TDC) by LeCroy permits much faster digitization than was possible with the previously used time-to-amplitude converter (TAC) followed by a PHA.

(2) Larger crystals with better reflectivity will provide larger count rates.

(3) It is contemplated to add small amounts of argon to the plasma, which gives higher count rates than iron at low electron temperatures.

(b) Several arms will operate in the XCS system simultaneously and provide radial profiles.

(c) Change of Bragg angle will be much more convenient in the present instrument, making it a much more versatile research instrument. This is so because crystals and detectors are moved independently and because less neutron shielding is required during d-d operation than for PDX, since the instrument is located in the diagnostic basement.

In order to put the TFTR X-ray diagnostic preparation into perspective, we conclude this paper with a very brief outlook on the X-ray diagnostics for the next larger generation of tokamaks (FED, INTOR or whatever their names may be). Of the three major X-ray diagnostics, only the crystal spectrometer can be used without major modification on these advanced machines. The PHA system has a problem with detector damage by neutrons. This problem may be avoided by replacing the Si(Li) detectors with gas-scintillation proportional counters (GSPC), sacrificing resolution /34/. The XIS system, as we have seen, is

insufficient for d-t operation even on TFTR. Considerable development and effort will be necessary to find alternative solutions for these two diagnostics.

TABLE I

	density g/cm^3	approx. cost $/lb	d-d** attenuation length in cm λ_s	d-d** attenuation length in cm λ_t	d-t** attenuation length in cm λ_s	d-t** attenuation length in cm λ_t
Water + 1% Boron	1.03	.02***	5.3	5.3	11.3	12.3
Polyethylene	.92		3.9	4.0	10.1	10.9
Polyethylene + 5% Boron	.95	3.50*	3.9	3.9	10.0	10.7
Gypsum Commercial	1.60	.15	9.3	9.5	13.1	15.1
Gypsium + 5% Boron	1.63	2.40*	9.0	9.1	12.7	14.5
Concrete,T4 (5% H_2O)	2.35	.20	10.5	12.0	10.5	14.1
Limestone Concrete (8% H_2O)	2.38	.20	9.9	10.0	10.2	12.5
80% Iron 20% Water	6.6				7.5	7.5

* e.g., RX203, RX283, respectively, from Reactor Experiments Inc., San Carlos, CA.

** The transport of neutrons is determined by the component with the smallest removal cross section which - exceptions excluded - is not too different from the removal cross section for the fastest component. The quoted lengths are the attenuation length of the 2.5-MeV and 14-Mev component, λ_{source} and the attenuation length of the total neutron flux, λ_{total}. The fast neutrons generate, however, a population of thermal and slow neutrons in the shield, and the total neutron flux is typically a factor 3-20 larger than the flux of the fast component. If the neutrons impinging on the shield are unmoderated, the slow and the thermal neutron populations have first to be generated, and the total neutron flux might actually increase for 2 or 3 attenuation lengths in the shield. Because of the large capture cross section of boron for thermal neutrons, addition of 1 to 2% boron eliminates effectively the thermal neutron population.

*** Manufacture of water tanks not included.

TABLE II

CROSS SECTION FOR 14 MEV NEUTRONS IN SILICON[13]

σ_{total}	1.8 barn
σ_{el} (n,n)	.8 barn
σ_{inel} (n,n')	.7 barn
σ (n,p)	.3 barn
σ (n,α)	.05 barn

Acknowledgments

The continuing support of Dr. H.P. Furth, Dr. P.M. Rutherford and Dr. D. Meade is gratefully acknowledged. Discussions with Dr. F. Goulding and his group, and with Dr. Radeka and his group were very helpful in clarifying many issues. We thank Drs. H. Hendel, L. Samuelson, and co-workers for helping us with experiments on the neutron generator. J. Gorman and T. Cost gave us excellent technical support. This work was supported by the United States Department of Energy Contract Number DE-AC02-76-CHO-3073.

References

[1]K.W. Hill, M. Bitter, D. Eames, S. von Goeler, N.R. Sauthoff, and E. Silver in Low Energy X-ray Diagnostics, AIP Conf. Proceedings No. 75, Ed. David T. Attwood and Burton L. Henke, (American Institute of Physics, New York) p. 8-24. (1981).

[2]S. von Goeler in Diagnostics for Fusion Experiments (Varenna), Ed. E. Sindoni and C. Wharton, Pergamon Press (1978).

[3]J.F. Baur et al., General Atomics report, GA-A16614 (1981).

[4]J. Strachan et al., Nucl. Fusion 21, p. 67 (1981).

[5]W.W. Engle Jr., "ANISN - A One Dimensional Discrete Ordinates Transport Code with Anisotropic Scattering," CCC-254, Radiation Shielding Information Center, Oak Ridge, TN. (1973).

[6]Detector-response calculations were done with IQCODE, a transport-response computer code provided by T. Jordan of Experimental and Mathematical Physics Consultants, Box 66331, Los Angeles, CA. 90066 (private communication).

[7]L.P. Ku, "Nuclear Radiation Analysis for TFTR," PPPL-1711, September (1980).

[8]E.H. Silver et al., Rev. Sci. Instr. 53, p. 1198 (1982).

[9]P. W. Nicholson, "Nuclear Electronics," J. Wiley & Sons (1974).

[10]Details of the Si(Li) X-ray detector system for TFTR and the electronics will be presented by D.A. Landis, N.W. Madden, and F.S. Goulding at the IEEE Nuclear Science Symposium, Washington, D.C., October 20-22, 1982.

[11]E.M. Lent, Lawrence Radiation Laboratory Livermore report UCRL-50857 (1970).

[12]R.A. Lillie, R. Alsmiller, J. Mihalczo, Nuclear Technology 43, 373 (1979).

[13]D.I. Garber and R.R. Kinsey, Neutron Cross Sections, Volume II, Brookhaven report BNL-325 (1976).

[14]D.I. Garber et al., Angular Distributions in Neutron-Induced Reactions, Vol. I, Brookhaven report BNL-400 (1970).

[15]A. Sattler, Phys. Rev. 138 A, p.1815, (1965).

[16]H.J. Stein, J. Appl. Physics 38, p. 204 (1967).

[17]D.W. Mingay et al., Nucl. Inst. and Methods 94, p. 497 (1971).

[18]G. Dearnaley, in "Progress in Fast Neutron Physics," Ed. G. Phillips, J.B. Marion, and J.R. Risser, University of Chicago Press pp. 173-192 (1963).

[19]D.A. Landis et al., Lawrence Radiation Laboratory Berkeley report LBL-13214 (1981).

[20]Y.M. Liu and J.A. Coleman, IEEE Trans. Nucl. Sci. NS-19, p.346 (1972).

[21]F. Goulding and R.H. Pehl, IEEE Trans. Nuc. Sci. NS-22, p.149 (1975).

[22]N. Sauthoff et al., Nucl Fusion 18, 1445 (1978).

[23]N. Sauthoff and S. von Goeler, IEEE Trans. Plasm. Sci. PS-7, p. 141 (1979).

[24]J.B. Reagan, "High Resolution Measurement of Space Radiation Effects on Silicon Surface-Barrier Detectors, "IEEE Trans. Nucl. Sci. NS-21, p.373 (1974).

[25]R.V. Babcock; IEEE Trans. Nucl. Sci. NS-8, p. 98 (1961).

[26]M. Goldman et al., Princeton report PPPL-1934 (1982) to be submitted to Rev. Sci. Instr.

[27]O. Frisch, British Atomic Energy Commission report BR49 (1949) (Unpublished).

[28]O. Bunemann, T.E. Cranshaw and J.A. Harvey, Can. J. Res. A27, p.191 (1949).

[29]David Eames, Ph.D. dissertation, Princeton (1980).

[30]S. von Goeler et al., "X-ray spectroscopy on tokamaks", lecture at this conference.

[31]K. Hill et al., Phys. Rev. A19, 1770 (1979)

[32]M. Bitter et al., Phys. Rev. Lett. 42, p. 304 (1979).

[33]M. Bitter et al., Proc. 6th Int. Symp. on Temperature, Washington, March 14-18, 1982, also Princeton report PPPL-1891 (1982).

[34]R.A. Boie et al., Brookhaven report BNL-30707 (1982), submitted to Nuc. Instr. Meth.

[35]A. Policarpo, Space Science Instrumentation 3, p.77-107 (1977).

Figure Captions

Fig. 1 Noise generated by neutrons in a Si(Li) detector on PLT. Subfigure a: Neutron emission as a function of time. Neutral-beam injection occurs from 400 to 600 ms. Subfigure b: Count rate of noise pulses generated by neutrons in the Si(Li) detector versus time. Subfigure c: Pulse-height spectrum of the neutron pulses measured during the time interval from 500 to 550 ms and added for 7 shots. The cut-off at low energy is produced by the discriminator of the amplifier. (#82X0595)

Fig. 2 Computation of the effectiveness of neutron shielding with the Jordan code /6/. Subfigure (a) is for a multiwire proportional counter; subfigure (b) is for a Si(Li) detector. The detectors are assumed to be shielded by 16 cm of lead and a layer of 32% borated polyethylene of variable thickness. Plotted is the reduction in neutron generated noise counts in the detector versus the thickness of the borated polyethylene. The various curves are computed for neutron and γ-ray fluxes which have been predicted for TFTR at a variety of locations shown in Fig. 3. The difference in attenuation between 5% and 32% boron is in general small, except in the basement, where the neutrons are highly moderated. (#82X0699)

Fig. 3 Neutron and γ-ray spectra computed for TFTR by Long-Poe Ku /7/. The spectra are calculated for various locations, which are labeled a, b, c, and which are marked in the subfigure on the lower right hand side. D-T stands for deuterium-tritium discharges producing 20 MW of

fusion power. D-D stands for deuterium-deuterium discharges with 22 kW of fusion power. The (d-d) reaction produces tritium, and a 2% d-t burn is consequently assumed for the D-D discharges, producing a sizeable peak of 14 MeV neutrons. In the D-D discharges, the igloo indicated in the subfigure on the lower right hand side is missing. The curves labeled c for the diagnostic basement have been calculated assuming that there exists a hole with a 3 foot diameter in the concrete below the center column. It is now planned to plug the hole, which will reduce the flux in the basement by another order of magnitude leaving the shape of the spectrum more or less unchanged, except for a reduction of the 14 MeV peak. (#82X0557)

Fig. 4 The figure illustrates the basic function of one channel of the (PHA) system. There are six channels on one arm. The photo shows the 6-detector cryostat built for TFTR by Lawrence Radiation Laboratory, Berkeley /10/. (#82X2300)

Fig. 5 Physical layout of the PHA system in the diagnostic basement of TFTR. The side view on the right hand side indicates 12 arms but shows details for only one. (#82X2260)

Fig. 6 The figure illustrates the basic function of one channel of the X-ray imaging system (XIS). The photo insert shows one of the surface-barrier-detector modules. (#82X0650)

Fig. 7 Physical layout of the X-ray imaging system (XIS) on TFTR. A vertical and a horizontal array consist each of two rows with 38

surface barrier detectors. Two of the detectors are shown magnified in the upper right hand corner with a steel tape in front of them carrying interchangeable absorber foils. In addition a movable detector (not shown) will be installed, that allows relative calibration of the detectors. (#82X2259)

Fig. 8 Gridded ionization chamber developed to replace surface barrier detectors during d-t operation /26/. Subfigure (a): Schematic drawing illustrating the function of the ionization chamber /27/28/: X-rays enter the chamber through the Be window on the left hand side and ionize the P10 gas. Ions are swept by the electric field to the cathode, electrons move to the grid and the anode. The grid functions as an electrostatic shield against image charges originating from ions. The anode collector current is due only to electrons. This feature provides fast time response (up to 1 MHz) for this type of ionization chamber. Subfigure (b): Mechanical parts for the gridded ionization chamber used for test purposes on PDX. Subfigure (c): Comparison of the signal output of a surface-barrier detector (upper trace) with that of a gridded ionization chamber (lower trace) during a disruptive discharge. (#82X0694)

Fig. 9 Schematic of a X-ray crystal spectrometer (XCS). (#773846)

Fig. 10 Physical layout of the planned TFTR X-ray crystal spectrometer (XCS). The crystals and detectors are housed in a large helium-filled chamber which is connected to the torus via two beryllium windows and two "see-thru" vacuum valves. The crystal-

detector distance is 5 m corresponding to a Rowland circle of approximately 3.5 m. The crystals will have an 8 cm x 20 cm reflecting area and consist of quartz (2243) or germanium (422) for the iron impurity, and of quartz (1120) for the argon impurity. The crystal mounting structure consists of a plane which permits mechanical movement of the crystal in the x-y direction and rotation. The detector for d-d operation consists of 10 cm x 18 cm multiwire proportional counters built by Brookhaven National Laboratory /33/. They have a position resolution of 400 μm and a countrate handling capability of 350 kHz. The detectors are shielded by 15 cm lead and 15 cm borated polyethylene. Special "Soller-slot" collimators reduce the radiation entering the detector enclosure through the X-ray aperture. The detector mounting structure permits x-y motion and rotation of the detector-shield assembly. (#82X0662)

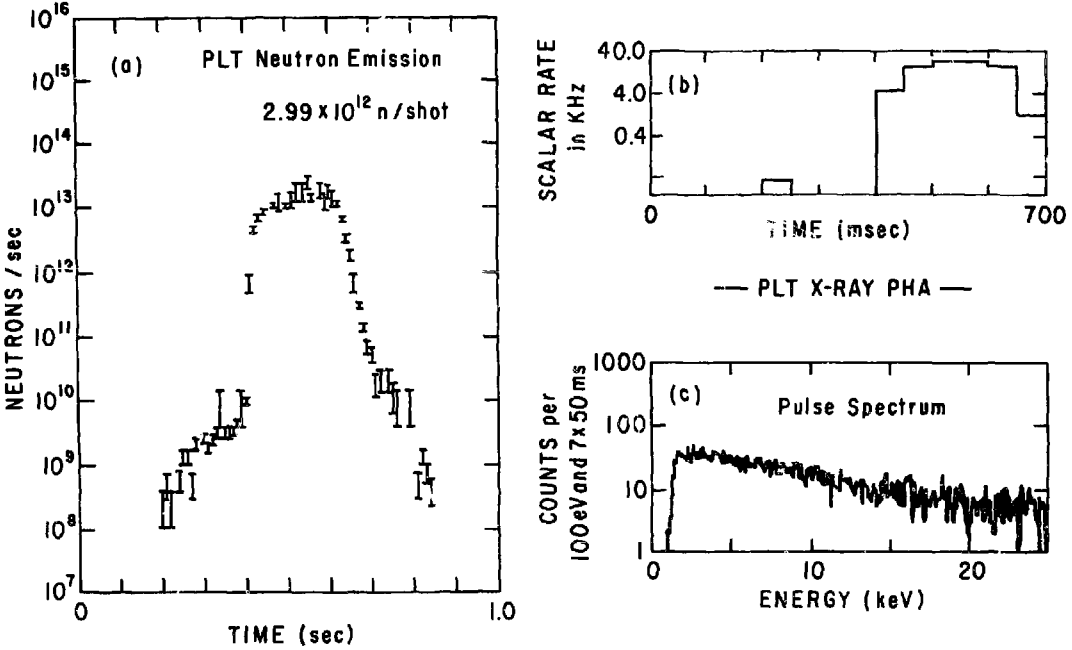
(a)
PLT Neutron Emission
2.99 x 10^12 n/shot
NEUTRONS / sec
TIME (sec)
(b)
SCALAR RATE in KHz
TIME (msec)
— PLT X-RAY PHA —
(c)
Pulse Spectrum
COUNTS per 100eV and 7x50ms
ENERGY (keV)

Fig. 1

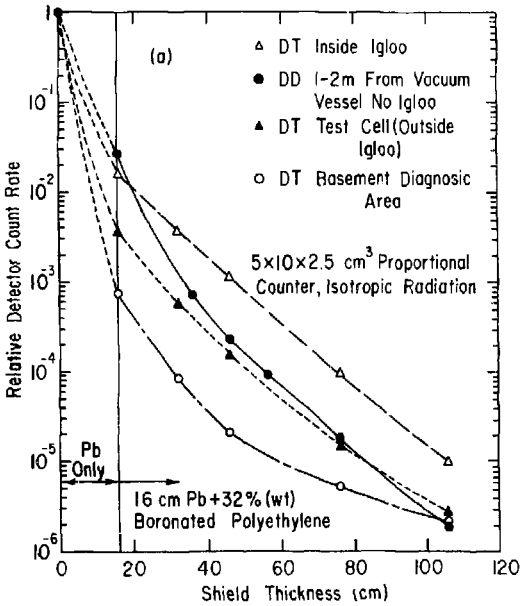
(a)
△ DT Inside Igloo
● DD 1-2m From Vacuum Vessel No Igloo
▲ DT Test Cell (Outside Igloo)
○ DT Basement Diagnosic Area
5×10×2.5 cm³ Proportional Counter, Isotropic Radiation
Pb Only
16 cm Pb+32% (wt) Boronated Polyethylene
Relative Detector Count Rate
Shield Thickness (cm)

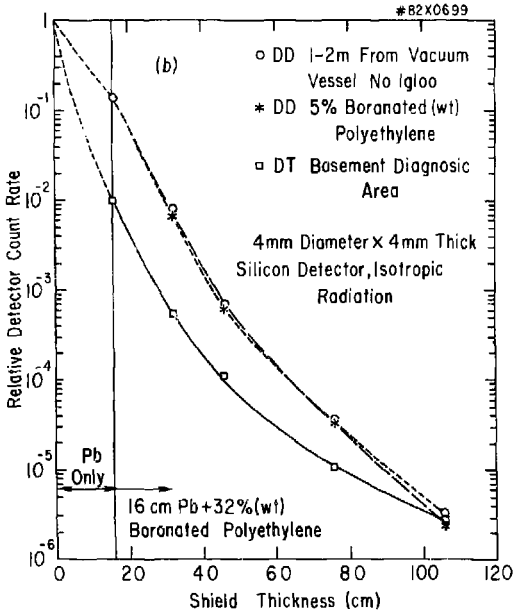
#82X0699
(b)
○ DD 1-2m From Vacuum Vessel No Igloo
* DD 5% Boronated (wt) Polyethylene
□ DT Basement Diagnosic Area
4mm Diameter × 4mm Thick Silicon Detector, Isotropic Radiation
Pb Only
16 cm Pb+32% (wt) Boronated Polyethylene
Relative Detector Count Rate
Shield Thickness (cm)

Fig. 2

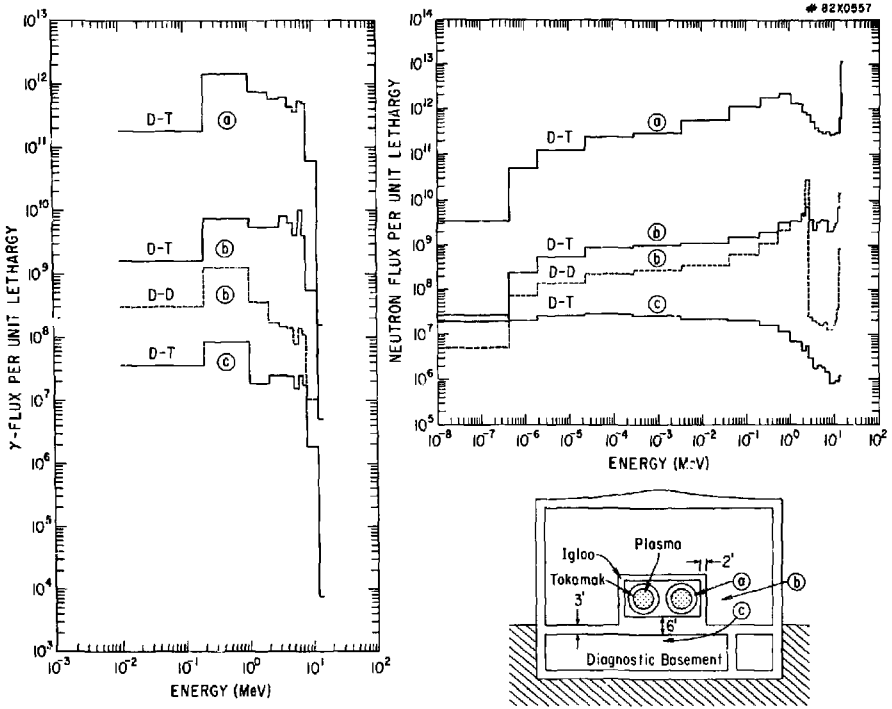
#82K0557
γ-FLUX PER UNIT LETHARGY
ENERGY (MeV)
D-T
D-T
D-D
D-T
NEUTRON FLUX PER UNIT LETHARGY
ENERGY (MeV)
D-T
D-T
D-D
D-T
Plasma
Igloo
Tokamak
2'
3'
6'
Diagnostic Basement

Fig. 3

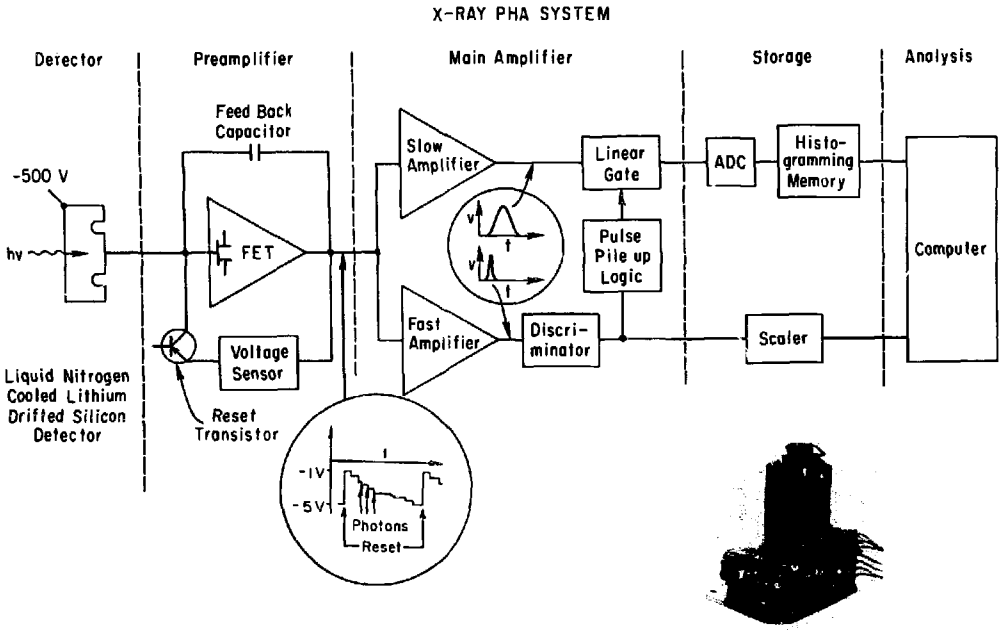
X-RAY PHA SYSTEM
Derector
Preamplifier
Main Amplifier
Storage
Analysis
Feed Back Capacitor
-500 V
hν
FET
Slow Amplifier
Linear Gate
ADC
Histo-gramming Memory
Computer
Pulse Pile up Logic
Fast Amplifier
Discri-minator
Scaler
Voltage Sensor
Liquid Nitrogen Cooled Lithium Drifted Silicon Detector
Reset Transistor
-1V
-5V
Photons
Reset

Fig. 4

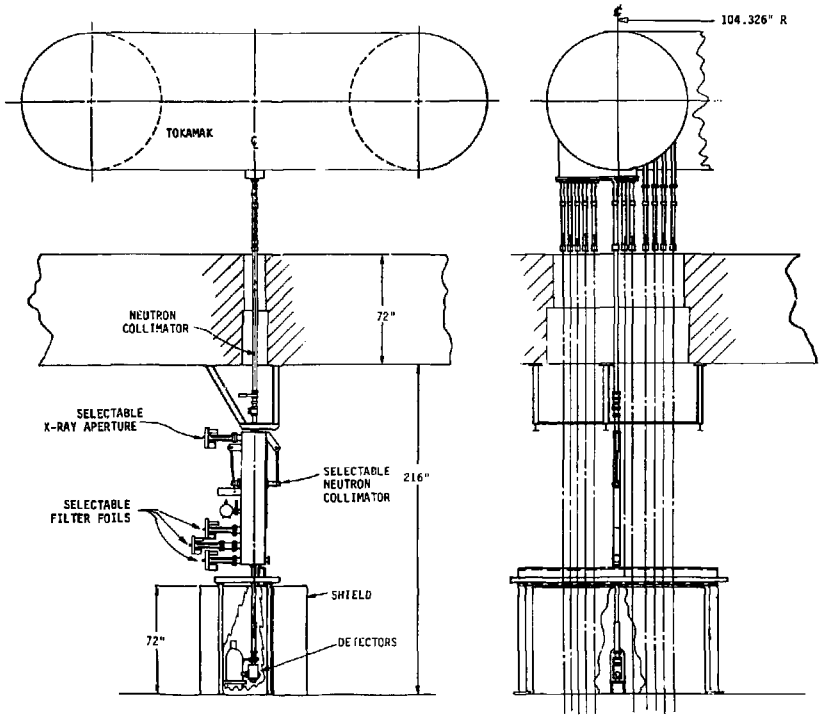
TOKAMAK
104.326" R
NEUTRON
COLLIMATOR
72"
SELECTABLE
X-RAY APERTURE
SELECTABLE
NEUTRON
COLLIMATOR
216"
SELECTABLE
FILTER FOILS
SHIELD
72"
DETECTORS

Fig. 5

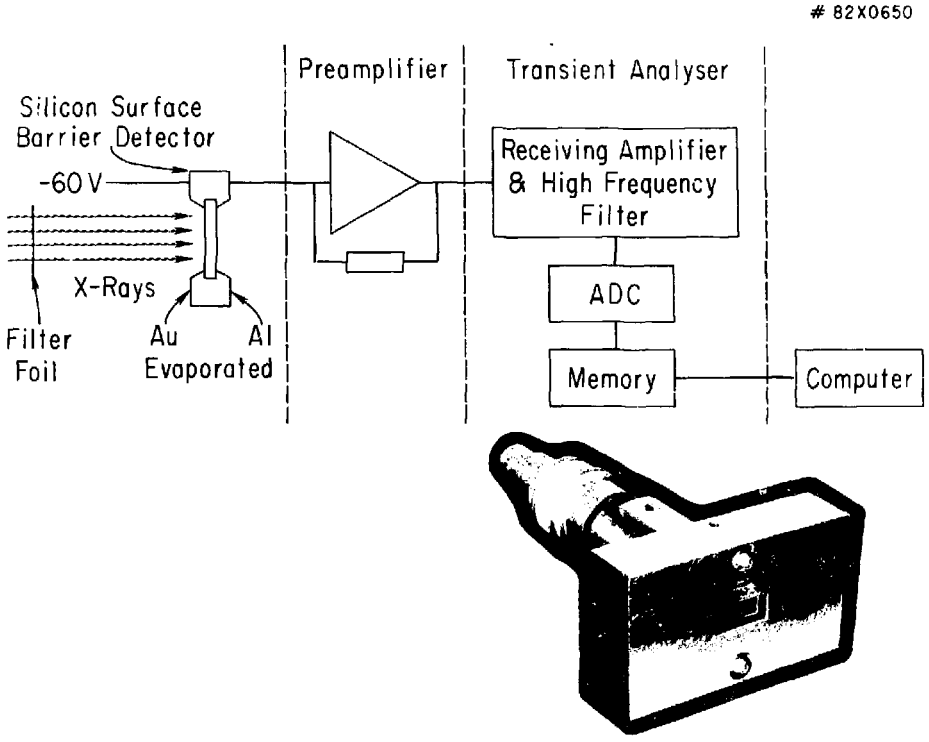
82X0650
Preamplifier
Transient Analyser
Silicon Surface
Barrier Detector
-60 V
X-Rays
Filter
Foil
Au
Al
Evaporated
Receiving Amplifier
& High Frequency
Filter
ADC
Memory
Computer

Fig. 6

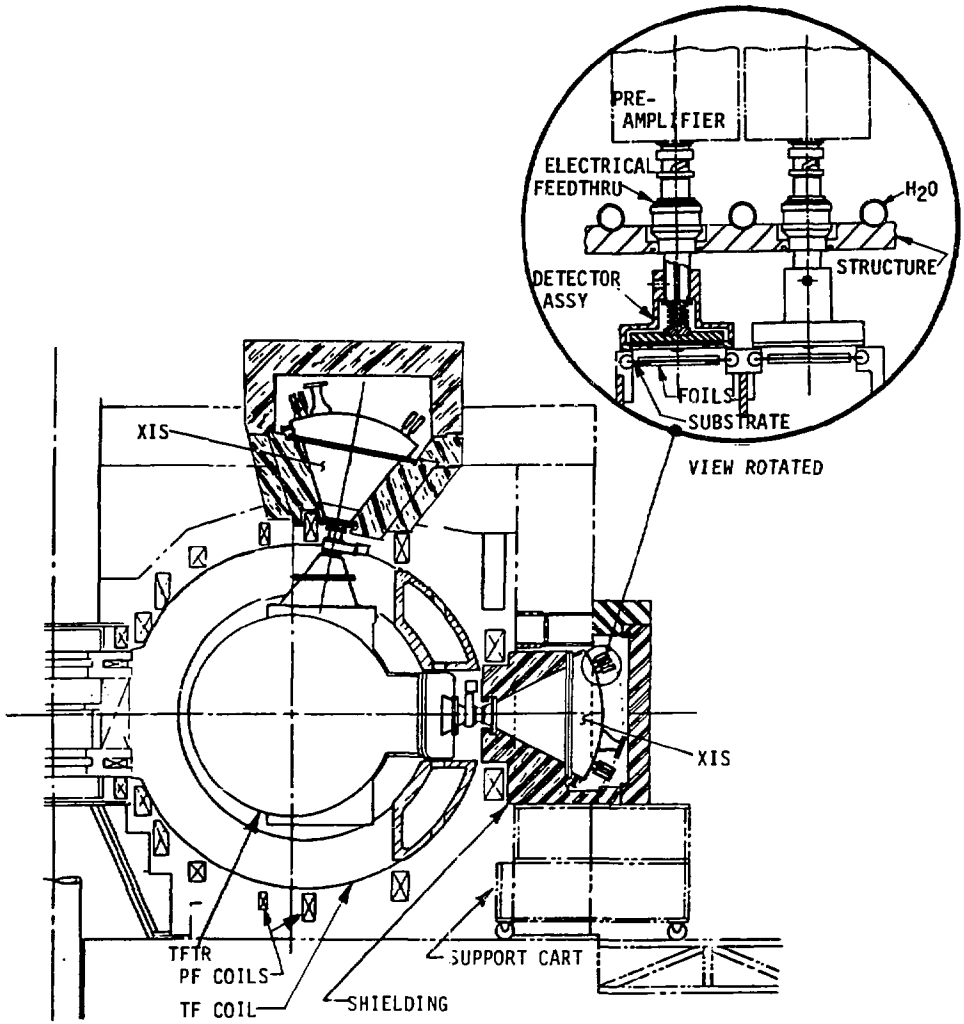
PRE-
AMPLIFIER
ELECTRICAL
FEEDTHRU
H_2O
STRUCTURE
DETECTOR
ASSY
FOILS
SUBSTRATE
VIEW ROTATED
XIS
XIS
TFTR
PF COILS
TF COIL
SHIELDING
SUPPORT CART

Fig. 7

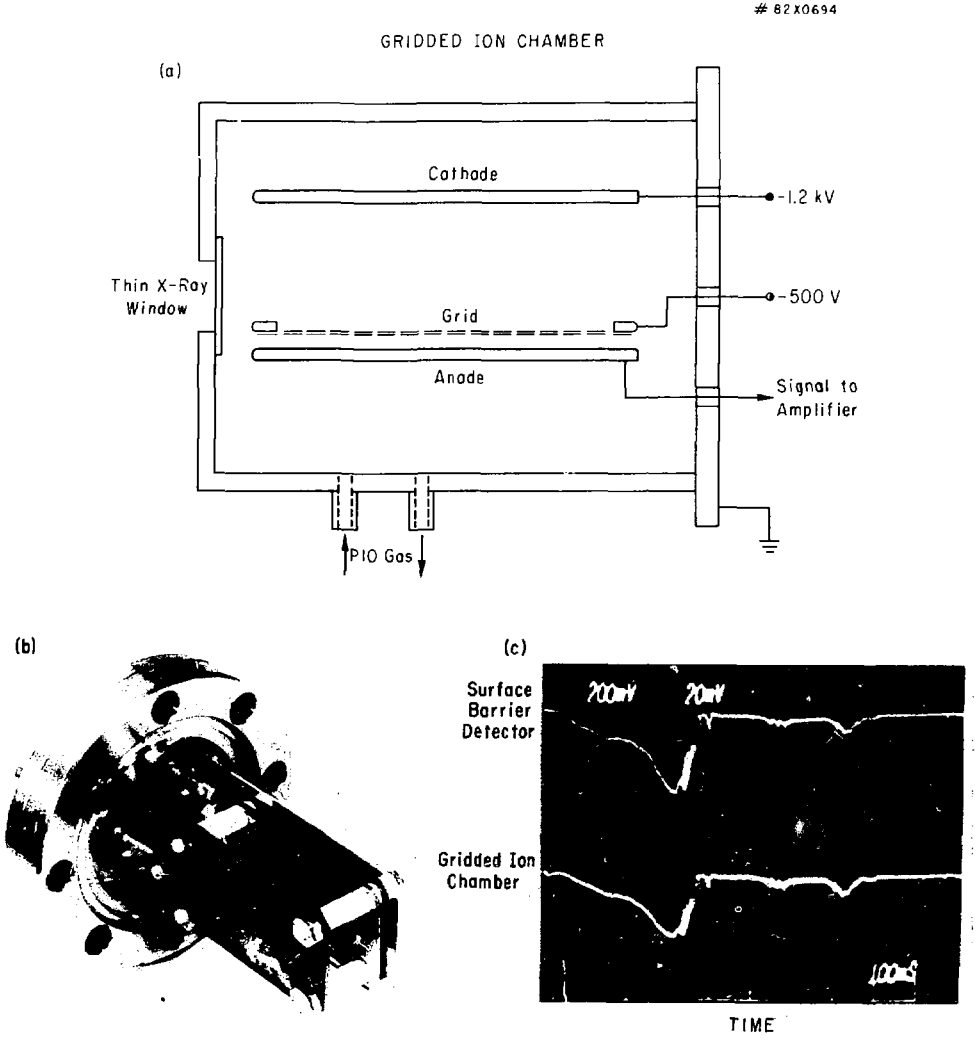
82X0694
GRIDDED ION CHAMBER
(a)
Cathode
-1.2 kV
Thin X-Ray Window
-500 V
Grid
Anode
Signal to Amplifier
P10 Gas
(b)
(c)
Surface Barrier Detector
Gridded Ion Chamber
TIME

Fig. 8

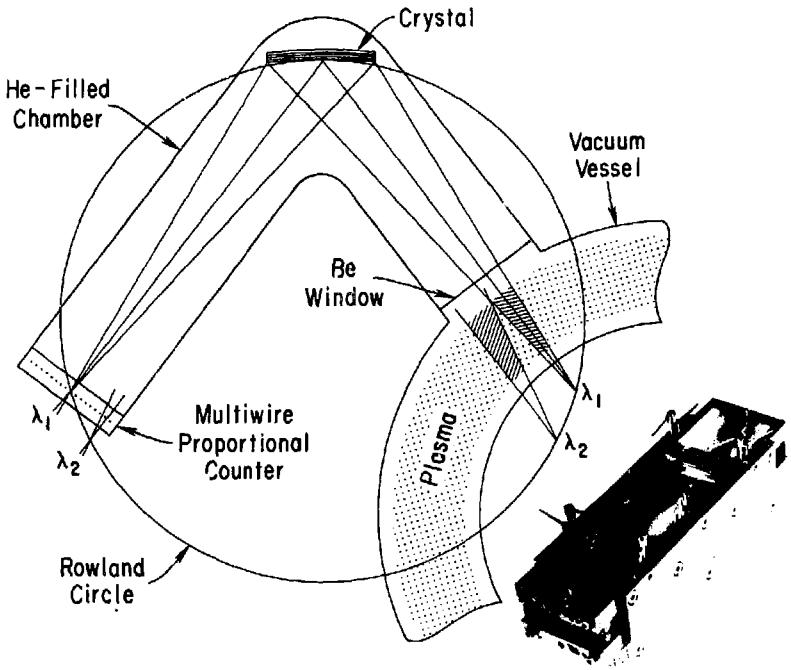
CURVED - CRYSTAL SPECTROMETER
Crystal
He - Filled Chamber
Vacuum Vessel
Be Window
λ_1
λ_2
Multiwire Proportional Counter
Plasma
Rowland Circle

Fig. 9

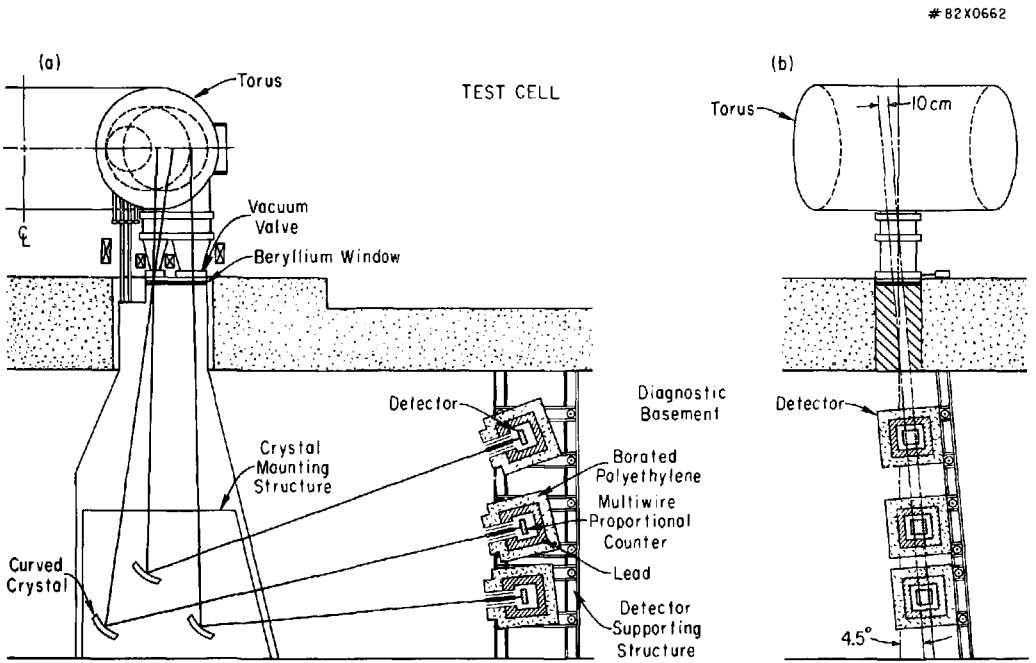
#82X0662
(a)
Torus
TEST CELL
Vacuum
Valve
Beryllium Window
Detector
Diagnostic
Basement
Crystal
Mounting
Structure
Borated
Polyethylene
Multiwire
Proportional
Counter
Lead
Curved
Crystal
Detector
Supporting
Structure
(b)
Torus
10cm
Detector
4.5°

Fig. 10